Supporting Information

Faïn et al. 10.1073/pnas.0905117106

SI Text

Latitudinal Distribution of Gaseous Elemental Mercury (GEM) Concentration During the Last 30 Years. Recent global modeling studies (1) suggest a latitudinal distribution of GEM concentrations in the Northern Hemisphere, with present levels slightly higher at 60°N. This present gradient is low (≈0.3 ng m^{-3}) (1). It is likely, however, that GEM levels in the Northern Hemisphere have been more heterogeneous in the past (i.e., in the 1970s and 1980s), as suggested by limited GEM observations onboard scientific ships in the Atlantic (2–5). Higher GEM emissions from anthropogenic sources may have strongly impacted temperate areas (i.e., 40–50°N) and to a lesser extent southern latitudes (i.e., 30°N and southern).

Ship-based records of atmospheric total gaseous mercury (TGM) represent the only data available in the late 1970s. TGM includes GEM and divalent gaseous mercury species; TGM and GEM could be assimilated here, as divalent gaseous mercury species represents only a few percent of TGM (ref. 6 and references therein). Fig. S1 presents a direct comparison of our reconstruction of atmospheric GEM inferred from firn air and the available onboard observations. Extreme caution is required when discussing ship-based records of atmospheric TGM. Such records are collected during short (i.e., multiweek) sampling periods, and thus are strongly influenced by short timescale variations of both natural and anthropogenic GEM sources. Fig. S1 suggests that the evolution of GEM concentrations reconstructed above Greenland cannot be generalized to the whole Northern Hemisphere but is instead likely to be representative of middle and high northern latitudes.

Parameterization of the Diffusion Model. We used a one-dimensional gas diffusion model in Eulerian coordinates (7) to infer the atmospheric record of GEM from firn air concentrations. We used firn structure parameters shown in Fig. S2 (density and closed porosity) from the EUROCORE drilling (8).

We determined GEM diffusivity in air at Summit Station, $D_{(T,P)}^{Surface}$, using the value reported by Massman (9) corrected for Summit temperature and pressure (8):

$$D_{(T,P)}^{Surface} = D_{T_0,P_0} \times {}^{P_0}/_{P} \times ({}^{T}/_{T_0})^{1.85} \quad [1]$$

where T_0 = 253.16 K, P_0 = 1013.25 mbar, T = 241 K, and P = 675 mbar. T and P are mean annual atmospheric values of temperature and pressure for the Summit site. Eq. **1** gives GEM diffusivity in the atmosphere above the firn surface. To obtain effective diffusivity of GEM in the firn, we used the following relation:

$$D_{eff} = {}^{\phi}/_{\tau} \times D_{(T,P)}^{Surface} \quad [2]$$

where ϕ is the snow porosity determined using the densities of snow and ice:

$$\phi = 1 - {}^{\rho_{Snow}}/_{\rho_{Ice}} \quad [3]$$

and τ is the firn tortuosity.

Tortuosity of a porous medium represents the complexity of the pathway and is commonly calculated as the ratio of the mean path length to the minimum possible (straight line) path length. Effective diffusivity of GEM depends on firn tortuosity, which increases progressively with depth. A null value of the ratio $1/\tau$ at the top of the lock-in zone means that diffusion ceases at this depth. In short, GEM effective diffusivity decreases from the snow surface value to zero at the close-off depth.

We used an inverse method (7, 10) to compute the ratio at all depths in the firn from the CO_2 atmospheric trend (Fig. S3*a*) and from CO_2 concentrations measured in the firn at Summit (Fig. S3*b*). In other words, we obtained a site-specific, diffusivity-depth relationship by adjusting diffusivity until the model reproduced the observed CO_2 firn-air profile when driven by the independently derived atmospheric CO_2 history. We sampled air for CO_2 analysis at the same depths as GEM. The CO_2 atmospheric scenario was derived from measured values from Alert, Canadian Arctic (11), Mauna Loa, Hawaii (12), and DE08 firn, Antarctica (13) records. We corrected records from Mauna Loa and DE08 from the difference between measured Alert and global concentrations.

Previous modeling studies (14–17) were able to reproduce accurately CO_2 concentrations measured in firn air at NGRIP (75°N, 42°W) using the CO_2 atmospheric history represented in Fig. S3*a*. The same studies simultaneously obtained similar results for various species (e.g., SF6, ref. 14), confirming the good parameterization of their models. NGRIP is a camp located on the Greenland ice sheet, a few hundred kilometers north of Summit, where firn air was sampled during July 2001. Thus, we considered that atmospheric evolution of CO_2 described previously was appropriate for parameterization of our diffusion model.

Validation of Model Parameterization. We validated parameterization of the ratio ϕ/τ using CH_4 and three halocarbon species (CFC11, CFC113, and CCl_4) for which atmospheric histories have been estimated from emission scenarios and real-time measurements (11, 18, 19). Concentration-depth profiles were determined for these four species using the adjusted ϕ/τ-depth profile in the diffusion model, and good agreement with concentration-depth profiles actually measured in the Summit firn was obtained (Figs. S4 and S5).

Changes in atmospheric concentrations of CFC11, CFC113, and CCl_4 during recent decades were ≈7%, ≈6%, and ≈11.5%, respectively, and these species poorly constrain the diffusivity profile in shallow firn. GEM concentrations have not exhibited important changes during the last 15 years, however, and our results were not sensitive to errors in diffusivity in the shallow firn.

Monte Carlo Modeling. We chose a mathematical parameterization of atmospheric GEM history from 1940 to 2006 (firn air model input)—which allowed for the possibility of a constant level, monotonic increase, or decrease, or peak concentration of GEM concentration during this timeframe, depending on the choice of parameter values. Specifically, we combined two log-normal functions to represent a potential peak in concentrations. We tested a wide range of parameter values with the forward firn air model previously described (Monte Carlo approach), representing widely varying scenarios for the atmospheric evolution of GEM concentrations. We then modeled a profile of GEM concentrations in the firn from each atmospheric history tested. Agreement between a modeled firn profile j and the experimental firn profile (Fig. 1) was estimated using the χ^2_j parameter defined by the following relation:

$$\chi_j^2 = \sum_{i-1}^{n} \left(\frac{(Hg^{\circ}_{Measured})_i - (Hg^{\circ}_{Modeled,j})_i}{\sigma_i} \right)^2 \quad [4]$$

where σ_i represents the measurement error associated with $(Hg°_{Measured})_i$. According to Tarantola theory (20), we were able to associate a probability density p_j with each atmospheric scenario tested (Eq. **5**), using the χ^2_j value previously determined:

$$p_j \propto \exp\left[-\frac{\chi_j^2}{2}\right] \quad [5]$$

We finally assessed probability distributions for GEM concentrations with a 1-year time resolution. Such distributions were obtained by a statistical analysis of all GEM atmospheric histories tested for any 1-year time interval:

$$p(x, x+dx) \propto \sum_{j\text{-}0}^{N} p_j \times \delta_j(x, x+dx) \quad [6]$$

where $p(x,x,+dx)$ is the probability that the atmospheric concentration of GEM is in the interval $[x,x+dx]$ and $\delta_j(x,x,+dx)$ is a function whose value is one when the concentration of scenario j is in the interval $[x,x+dx]$ and zero otherwise. We calculated means and standard deviations from all distributions (i.e., every year from 1940 to 2006). The envelope of atmospheric GEM concentrations presented in this study corresponds to the mean concentrations plus or minus one standard deviation. Our Monte Carlo approach led to high quality results, but was time-consuming due to the large number of tested scenarios. Thus, inverse modeling should be considered as a potential improvement for further studies involving modeling of GEM diffusion processes in polar firn.

1. Selin NE, et al. (2007) Chemical cycling and deposition of atmospheric mercury: Global constraints from observations. *J Geophys Res* 112:D02308.
2. Slemr F, Junkermann W, Schmidt RWH, Sladovic R (1995) Indication of change in global and regional trends of atmospheric mercury concentrations. *Geophys Res Lett* 22:2143–2146.
3. Slemr F, Langer E (1992) Increase in global atmospheric concentrations of mercury inferred from measurements over the Atlantic Ocean. *Nature* 355:434–437.
4. Slemr F, Schuster G, Seiler W (1985) Distribution, speciation, and budget of atmospheric mercury. *J Atmos Chem* 3:407–434.
5. Temme C, Slemr F, Ebinghaus R, Einax JW (2003) Distribution of mercury over the Atlantic Ocean in 1996 and 1999–2001. *Atmos Environ* 37:1889–1897.
6. Fitzgerald WF, Lamborg CH, Hammerschmidt CR (2007) Marine biogeochemical cycling of mercury. *Chem Rev* 107:641–662.
7. Rommelaere V, Arnaud L, Barnola J-M (1997) Reconstructing recent atmospheric trace gas concentrations from polar firn and bubbly ice data by inverse methods. *J Geophys Res* 102:30 069–030 083.
8. Schwander J, et al. (1993) The age of the air in the firn and the ice at Summit, Greenland. *J Geophys Res* 98:2831–2838.
9. Massman WJ (1999) Molecular diffusivities of Hg vapor in air, O_2 and N_2 near STP and the kinematic viscosity and thermal diffusivity of air near STP. *Atmos Environ* 33:453–457.
10. Fabre A, Barnola J-M, Arnaud L, Chappellaz J (2000) Determination of gas diffusivity in polar firn: Comparison between experimental measurements and inverse modeling. *Geophys Res Lett* 27:557–560.
11. WDCGG (2006) in *http://gaw.kishou.go.jp/wdcgg/*.
12. Keeling CD, Whorf TP (1998) Atmospheric CO_2 concentration at Mauna Loa Observatory, Hawaii, 1958–1997. *Carbon Dioxide Inf Anal Cent, Oak Ridge Natl Lab, Oak Ridge, TN.*
13. Etheridge DM, et al. (1996) Natural and anthropogenic changes in atmospheric CO2 over the last 1000 years from air in Antarctic ice and firn. *J Geophys Res* 101:4115–4128.
14. Reeves CE, et al. (2005) Trends of halon gases in polar firn air: implications for their emission distributions. *Atmos Chem Phys* 5:2055–2064.
15. Worton DR, et al. (2007) Atmospheric trends and radiative forcings of CF4 and C2F6 inferred from firn air. *Environ Sci Technol* 41:2184–2189.
16. Worton DR, et al. (2006) 20th century trends and budget implications of chloroform and related tri-and dihalomethanes inferred from firn air. *Atmos Chem Phys* 6:2847–2863.
17. Bernard S, et al. (2006) Constraints on N_2O budget changes since pre-industrial time from new firn air and ice core isotope measurements. *Atmos Chem Phys* 6:493–503.
18. Etheridge DM, Steele LP, Francey RJ, Langenfelds RL (1998) Atmospheric methane between 1000 AD and present: Evidence of anthropogenic emissions and climatic variability. *J Geophys Res* 103:15979–15993.
19. Martinerie P, et al. (2009) Long-lived halocarbon trends and budgets from atmospheric chemistry modelling constrained with measurements in polar firn. *Atmos Chem Phys* 9:3911–3934.
20. Tarantola A (1987) *Inverse Problem Theory: Method for Data Fitting and Model Parameter Estimation* (Elsevier, New York).

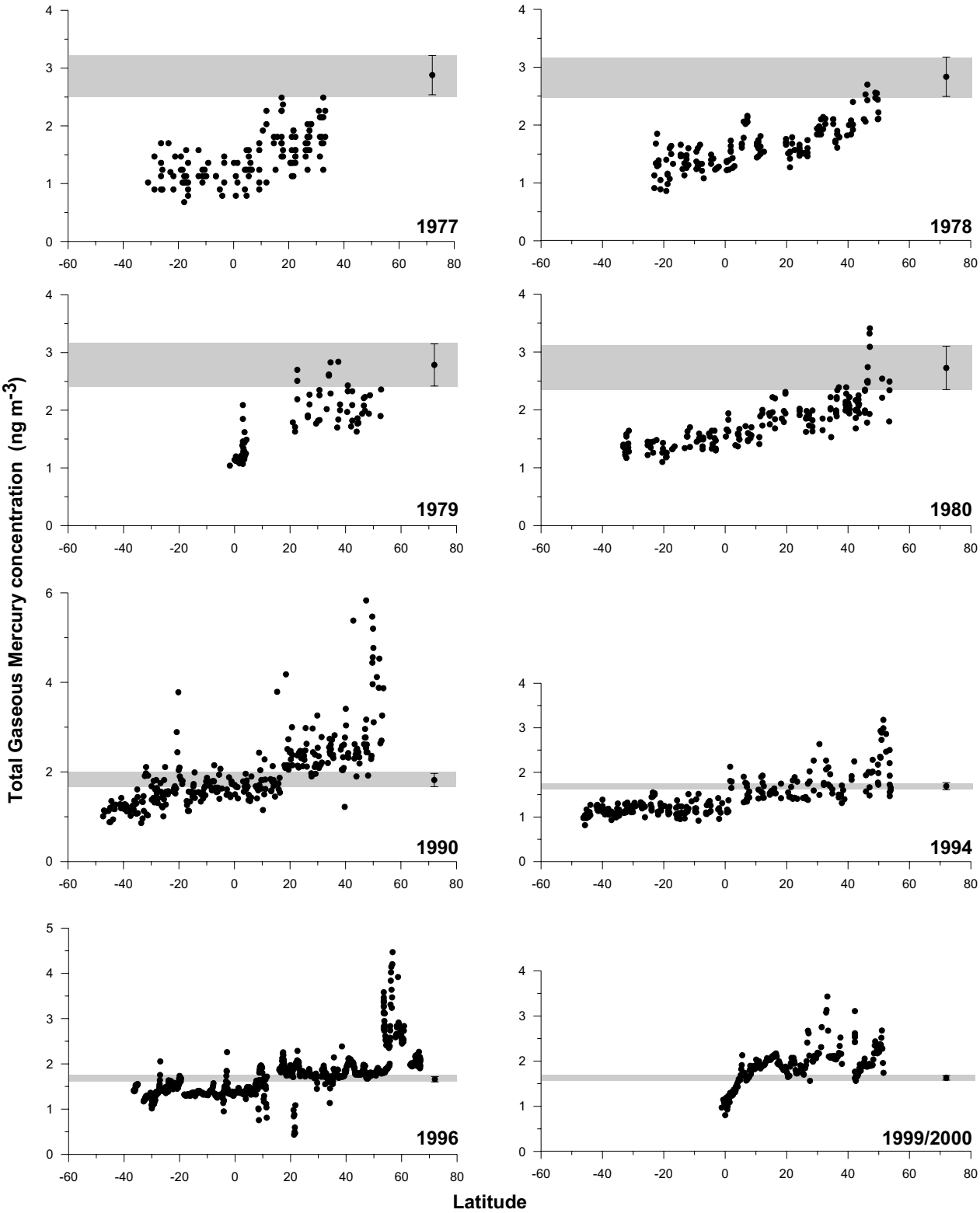

Fig. S1. Intervals of modeled concentrations for atmospheric GEM inferred from Summit firn air (gray stripes), and latitudinal distributions of total gaseous mercury (TGM) over the Atlantic for the years 1977, 1978, 1979, and 1980 (18), 1990 (17), 1995 (16), 1996, and 1999/2000 (19). TGM includes GEM and divalent gaseous mercury species.

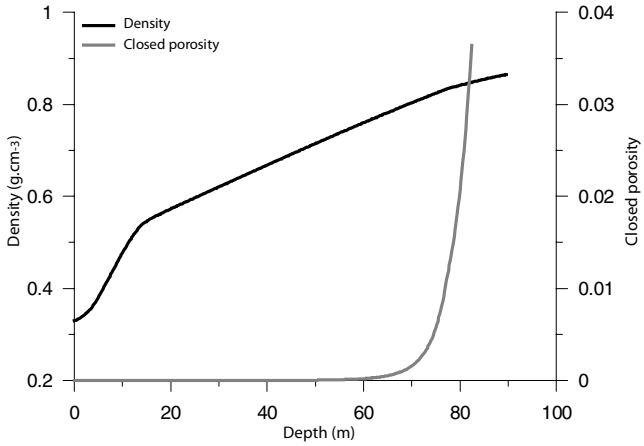

Fig. S2. Evolution of density and closed porosity with depth at Summit, Greenland (from ref. 8).

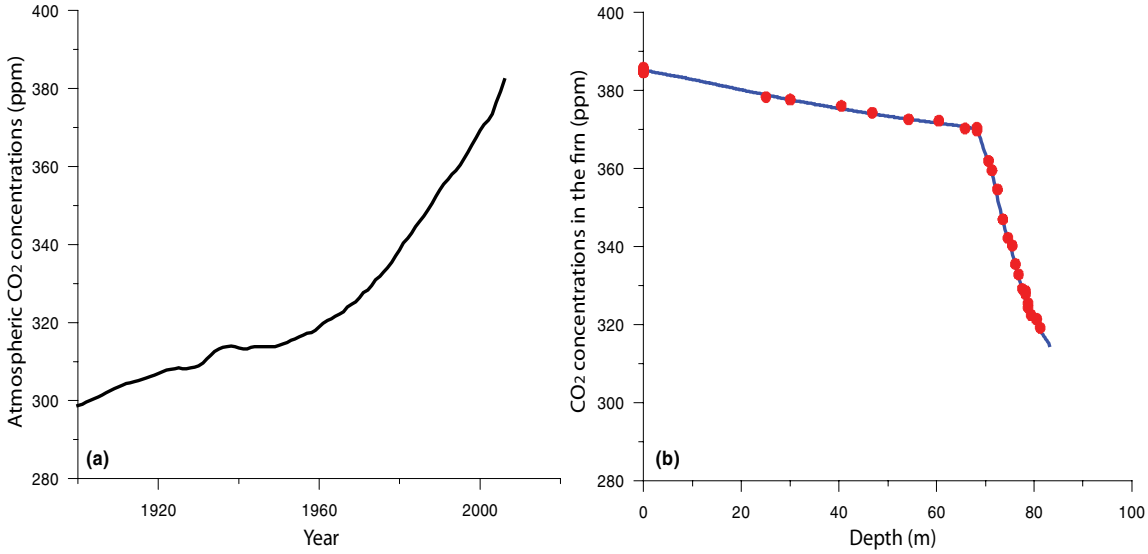

Fig. S3. (*a*) Atmospheric evolution of CO_2 during the last century, and (*b*) CO_2 concentrations measured in firn at Summit in June 2006 (red dots). The blue line represents the CO_2 firn profile modeled after adjustment of the ratio ϕ/τ (*b*).

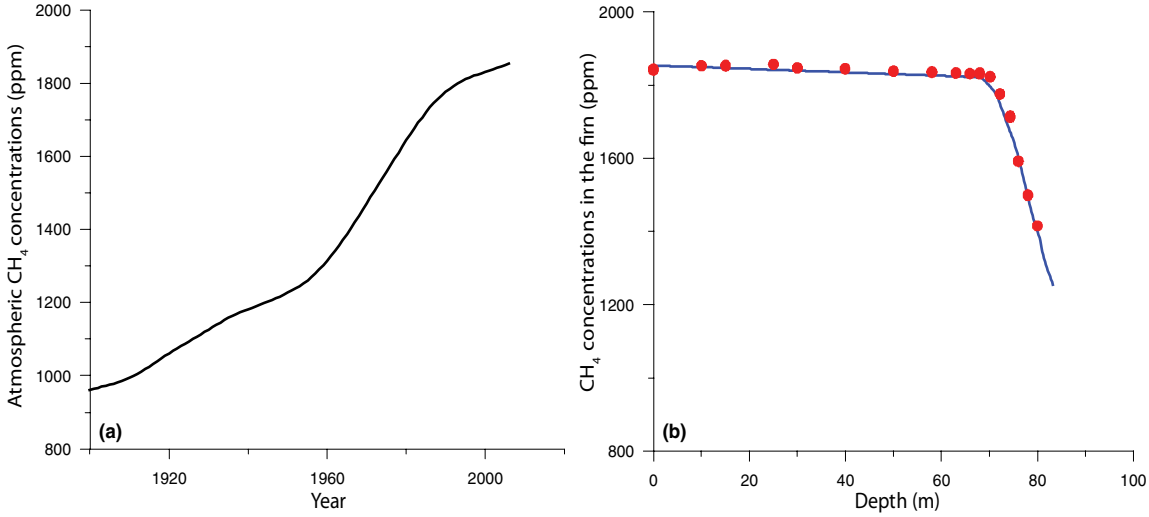

Fig. S4. (*a*) Atmospheric concentrations of CH_4 during the last century; (*b*) CH_4 concentrations measured (red dots) and modeled (blue line) in the firn at Summit after parameterization of the model.

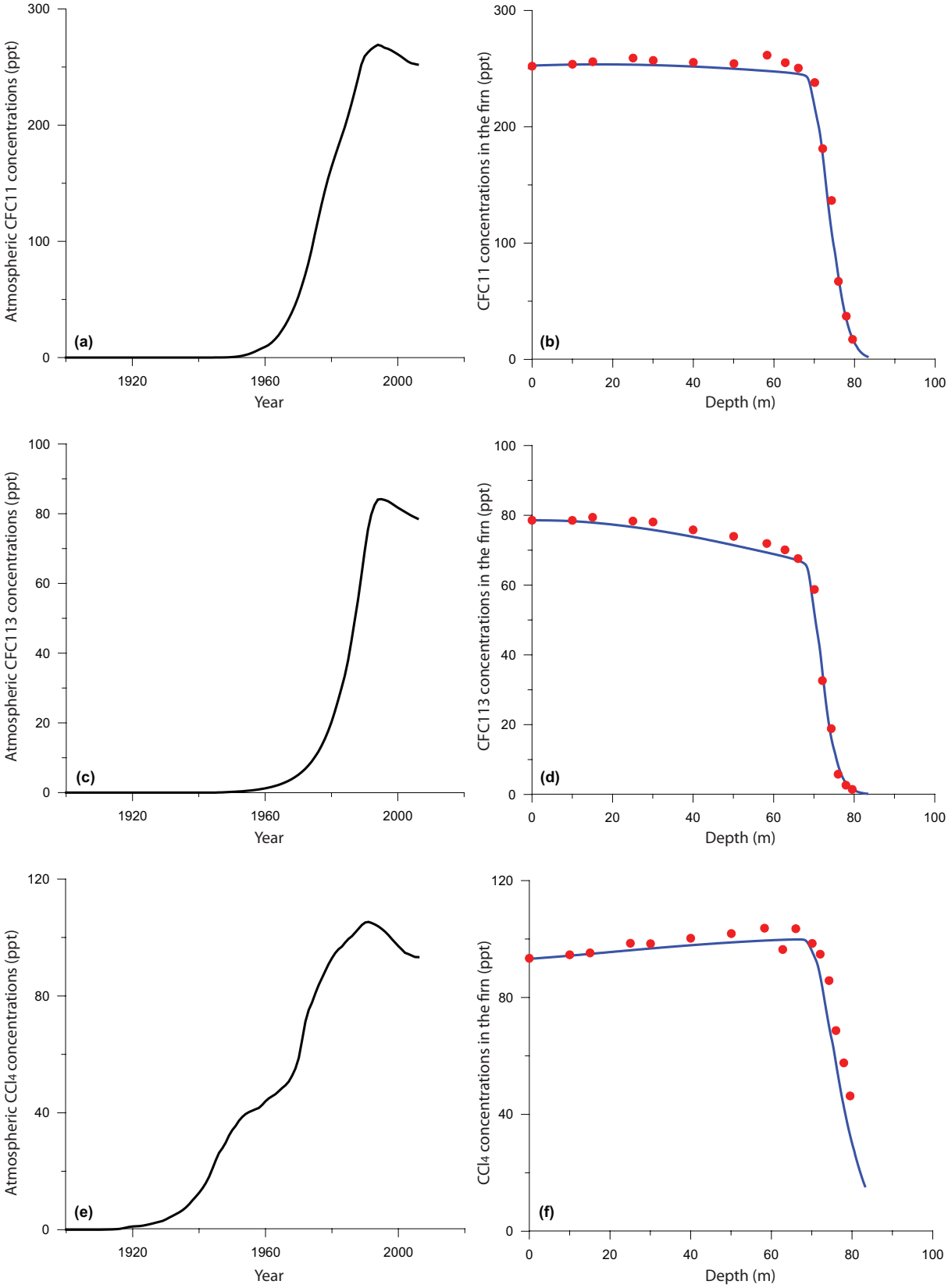

Fig. S5. Atmospheric concentrations of CFC11(*a*), CFC113 (*c*), and CCl_4 (*e*) (13); concentrations of these halocarbons measured (red dots) and modeled (blue line) in the firn at Summit after parameterization of the model (*b*, *d*, and *f*).